Rate-dependent adhesion of viscoelastic contacts. Part II: Numerical model and hysteresis dissipation

Rate-dependent adhesion of viscoelastic contacts. Part II: numerical model and hysteresis dissipation

G. Violano,[1] A. Chateauminois,[2] and L. Afferrante[1,*]

[1]*Department of Mechanics, Mathematics and Management, Polytechnic University of Bari, Via E. Orabona, 4, 70125, Bari, Italy*

[2]*Soft Matter Science and Engineering Laboratory (SIMM), PSL Research University, UPMC Univ Paris 06, Sorbonne UniversitÃ©s, ESPCI Paris, CNRS, 10 rue Vauquelin, 75231 Paris cedex 05, France*

Abstract

In this paper, we propose a numerical model to describe the adhesive normal contact between a glass spherical indenter and a viscoelastic model rough substrate of PDMS material. The model accounts for dissipative process under the assumption that viscoelastic losses are localized at the (micro)-contact lines. Numerical predictions are then compared with experimental measurements, which show a strong adhesion hysteresis mostly due to viscous dissipation occurring during pull-off. This hysteresis is satisfactorily described by the contact model which allows to distinguish the energy loss due to material dissipation from the adhesion hysteresis due to elastic instability.

Our analysis shows that the pull-off force required to detach the surfaces is strongly influenced by the detachment rate and the root mean square (rms) roughness amplitude, but it is almost unaffected by the maximum load from which unloading starts. Moreover, the increase in the length of the boundary line separating contact and non-contact regions, which is observed when moving from smooth to rough contacts, negligibly affects the viscous dissipation. Such increase is much less significant than the reduction in contact area, which therefore is the main parameter governing the strong decrease in the effective surface energy for the specific rough geometry considered in the present work.

Keywords: viscoelasticity, adhesion hysteresis, surface roughness, pull-off force.

*Electronic address: guido.violano@poliba.it

Introduction

Fuller and Tabor (FT) (1975) first showed that the pull-off force, i.e., the tensile load required to detach two contacting bodies, is strongly reduced when the surface roughness is increased. More recently, Persson and Tosatti (2001) found that adhesion leads to an increase in the real contact area, even when no pull-off force is detected.

Adhesive interactions are predominant at the nanometer scale for bodies and systems with a high surface to volume ratio. However, adhesion is still observed at macroscopic scales when the contacting bodies are soft. Typical examples are pressure sensitive adhesives (PSA) (Benedek, 2004), soft rubbers (Barthel and Frétigny, 2009), and biomimetic devices (Bauer et al., 2015).

In several experiments (Maugis and Barquins, 1978; Tiwary et al., 2017), the detachment behaviour of soft matter is found to be rate-dependent as a result of the intrinsic viscoelasticity of the material. In such conditions, the effective work of adhesion $\Delta\gamma_{\text{eff}}$ may be strongly increased compared to the quasi-static value $\Delta\gamma_0$ (see also Menga et al., 2018). Moreover, hysteretic energy dissipation can occur during contact loading-unloading loops. In this regard, Wei et al. (2010) found that roughness-induced adhesion hysteresis depends on a dimensionless adhesion parameter, which represents the statistical average of the repulsive forces due to elastic energy and the attractive ones due to the adhesive interactions. Deng and Kesari (2019) developed an analytical model that, under the assumption of large roughness, predicts a linear increase of the hysteretic dissipation with the area of contact. Moreover, Carbone et al. (2015), by numerical calculations performed on 1D self-affine fractal profiles, found there are two sources of energy dissipation, one at small scales and the other at large scales.

The contact between soft media is often described by the classical theory of adhesion of Johnson, Kendall and Roberts (JKR) (Johnson et al., 1971). However, JKR theory applies to purely elastic media as it neglects rate-dependence.

The coexistence of adhesion, viscoelasticity and surface roughness has been experimentally investigated in numerous works (Tiwary et al., 2017; Lorenz et al., 2013; Dorogin et al., 2018). In such works, loading-unloading experimental curves are usually fitted by exploiting JKR theory, with the stratagem of using different values of the work of adhesion and elastic modulus for the loading and unloading phases, respectively.

In the literature, there is a lack of analytical and numerical models aimed at describing the adhesive contact of viscoelastic bodies in presence of surface roughness. Haiat and Barthel (2007) proposed an approximate model for the contact of viscoelastic rough surfaces based on Greenwood and Williamson (GW) model (Greenwood and Williamson. 1966). From an experimental perspective, elucidation and validation of these models using microscopic randomly rough surfaces such as abraded or bead blasted surfaces is compromised by the difficulties in the measurement of the actual distribution of micro-contact areas at the micrometer scale.

In Violano et al. (2021), we experimentally studied the detachment of a rigid indenter from soft PolyDiMethylSiloxane (PDMS) substrates with smooth and rough surfaces. Specifically, roughness was obtained by texturing the surface with spherical identical microasperities with controlled height and spatial distributions. The designed patterned surfaces allow for a precise determination of the real contact area from micro-contact visualization. Interestingly, we found simple scaling laws relating the contact radius a and the contact line velocity v_c measured at the macro and microscales.

Moving from the observed similarity between macro and microscale contacts, we develop a numerical model aimed at describing both the loading and unloading phases occurring in typical JKR tests on rough samples. Specifically, the model exploits a discrete version of FT multiasperity model (Fuller and Tabor, 1975) to simulate the loading phase. The unloading phase is instead modelled on the basis of the solution proposed by Muller (Muller, 1999), with the assumption that the parameters of Muller's model, which are experimentally identified at the macroscale, can be applied to the microscale as they correspond to similar contact line velocities v_c.

I. EXPERIMENTAL SET-UP

For details about the experimental setup, the manufacturing of the PDMS samples and the experimental procedure used during indentation tests we refer the reader to Violano et al. (2021). Here, we simply summarize some aspects regarding the generated patterned surfaces.

Roughness on the top of PDMS samples is obtained by texturing them with identical spherical microasperities with controlled height and spatial distributions. Patterned surfaces

were obtained by moulding PDMS in PolyMethylMethAcrylate (PMMA) micro-milled forms using ball-end mills with a radius of 100 μm. In order to reduce the microscale roughness induced by the milling process and thus to enhance adhesion, the spherical cavities of the PMMA molds have been exposed to a saturated CHCl3 vapor for 30 minutes. As a result of the surface plasticization of the glassy acrylate polymer, surface tension effects were previously found to result in a smoothening of the surface of the spherical cavities of the mold (Acito et al. 2019). As a consequence, an increase in the radius of the spherical bumps is observed up to a 10% of the nominal value.

The size of these micro-asperities allows for an optical detection of the individual micro-contact areas, which in turn provides the relationship between the actual contact area A and the applied normal force F.

The patterned surfaces are generated with a squared nominal area of 10 mm^2, where asperities are randomly distributed with a density of 2×10^7 m^{-2}. Asperities are collocated with a non-overlapping constraint.

The first pattern is a regular square network of spherical caps having all the same height of 40 μm; the other patterns are characterized by spherical caps with heights distributed according to Gaussian distributions with standard deviations $\sigma = 5$ μm and $\sigma = 10$ μm, respectively.

Indentation experiments of the glass lens on the smooth part of the PDMS sample were performed at increasing loads and the contact radius was measured at each load step after a time of 800 s, which is large enough to achieve the adhesive equilibrium with viscoelastic effects totally dissipated (Acito et al., 2019). The resulting contact radius vs. load data were fitted according to JKR theory. The fit allows to estimate the values of the reduced elastic modulus ($E^* = 0.83$ MPa) and adhesion energy ($\Delta\gamma_0 = 0.037$ J/m^2).

The experimental tests on the rough patterns are performed in 6 different locations for each pattern in order to have 6 realizations of the surface topography.

During the loading phase, contact tests are performed under controlled load conditions. The applied load is increased step by step of 4 mN and, during each step, the indenter approaches the PDMS substrate with a velocity $V = 0.5$ μm/s. Unloading tests are instead performed by controlling the driving velocity. In such case, viscous effects occur during the detachment process and JKR theory is no longer valid.

II. NUMERICAL MODEL

Figure 1A shows the frictionless adhesive contact between a 'rigid' indenter and a soft substrate of PDMS material textured with spherical micro-asperities of identical radii of curvature.

As above explained, the loading process was executed experimentally under conditions of adhesive equilibrium. Viscoelasticity is hence negligible and micro-asperities were modeled as elastic spheres in the simulation. Conversely, viscous dissipation is no longer negligible during the unloading phase. Here, the problem is treated under the assumption that viscoelastic losses are restricted to the contact line while the bulk of the micro-contact zone behaves elastically.

This hypothesis is supported by the low glass transition temperature of the used silicone ($T_g \approx -120$ °C). For our PDMS, the frequency for glass transition at room temperature is about 10^8 Hz. Such frequency was measured by Dynamic Mechanical Thermal Analysis (DMTA) using a classical master curve methodology based on a time-temperature equivalency. Storage and dissipative components of the shear modulus G^* were measured at various temperatures (from -77 °C to 23 °C) and frequencies (from 0.01 to 50 Hz). The obtained master curve indicates that the glassy region is achieved above the maximum achievable frequency, i.e., 10^8 Hz at 21 °C. Moreover, the loss modulus is about 10 times lower than storage one (i.e., $\tan\delta < 0.1$) up to 10 Hz, which is the maximum strain frequency for the bulk of the micro-asperity contacts in our study. In fact, a very rough estimate of the exciting frequency at the level of micro-contacts is $\sim v_c/a$, where $v_c = -da/dt$ is the contact line velocity and a the radius of micro-spots. As v_c is estimated $< 10^{-4}$ m/s, assuming that a takes on average values of the order of 10^{-5} m, we have exciting frequency less than 10 Hz. Such value confirms that viscoelastic losses are negligible within the bulk of micro-asperity contacts as we are moving inside the rubbery region (or at most on the border with the transition region).

A. Loading phase

Numerical simulations of the loading phase are performed by using a discrete version of FT multiasperity model, where the geometry of each asperity is calculated instead of using

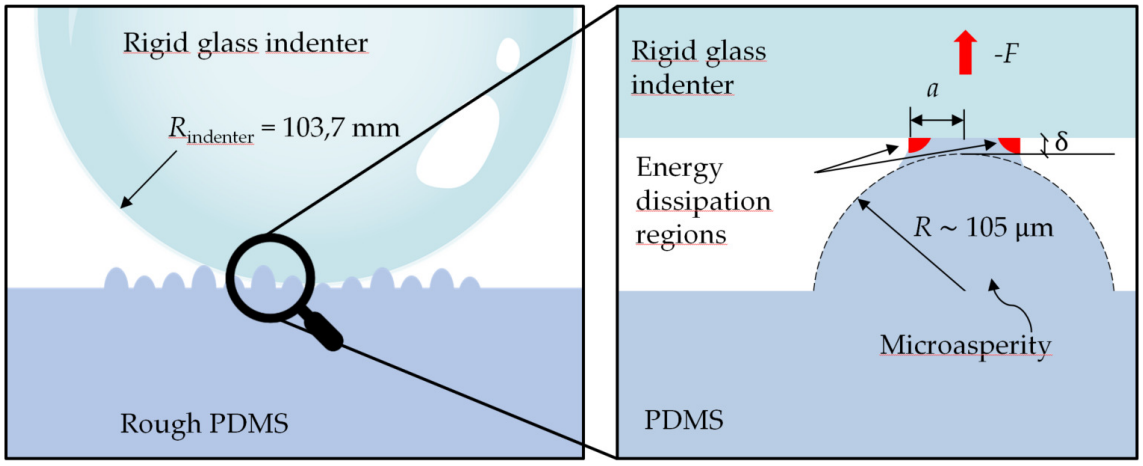

FIG. 1: The problem under investigation: the normal adhesive contact between a rigid smooth spherical lens and soft rough PDMS. In the zoom, detachment of a microasperity occurs under a tensile (negative) load F.

a statistical distribution of heights.

Each micro-asperity behaves as an isolated contact punch and, according to JKR formalism (Johnson et al., 1971), the contact load F and penetration δ are given by

$$F = \frac{4}{3}\frac{E^* a^3}{R} - \sqrt{8\pi E^* \Delta\gamma_0 a^3} \tag{1}$$

$$\delta = \frac{a^2}{R} - \sqrt{\frac{2\pi a \Delta\gamma_0}{E^*}}, \tag{2}$$

where E^* is the reduced elastic modulus and a and R are the contact radius and radius of curvature (see Fig. 1).

The total contact area and total applied load are obtained by summing up the contributions of each contacting asperity. For each set of surface and contact parameters, five numerical realizations of the surfaces were considered.

In this model, the lateral interaction between asperities is not taken into account as elastic coupling can be reasonably neglected for the considered surfaces (Acito et al., 2019; Yashima et al., 2015). However, we stress that lateral interaction is instead of crucial importance when the surfaces are characterized by roughness distributed on several length scales (Violano and Afferrante, 2019a; Violano and Afferrante, 2019b).

B. Unloading phase

Simulations of the unloading phase are performed on the basis of the solution proposed by Muller (Muller, 1999) and just exploited in Violano and Afferrante (2019c). Muller showed that the detachment process of a rigid sphere from a viscoelastic half-space can be described by a two-parameter differential equation, which in dimensionless form writes

$$\frac{d\bar{a}}{d\bar{\delta}} = \left[\frac{\Delta\gamma_0}{RE^*}\right]^{1/3} \cdot \frac{1}{\beta}\left[\bar{a}^3\left(1-\frac{\bar{\delta}}{3\bar{a}^2}\right)^2 - \frac{4}{9}\right]^{1/n}, \tag{3}$$

where $\bar{a} = a/a_0$ and $\bar{\delta} = \delta/\delta_0$, with $a_0 = 3R\left[\pi\Delta\gamma_0/(6E^*R)\right]^{1/3}$ and $\delta_0 = 3R\left[\pi\Delta\gamma_0/(6E^*R)\right]^{2/3}$. The parameter β is given by

$$\beta = \left(\frac{6}{\pi}\right)^{1/3}\left(\frac{4}{9}c\right)^{1/n} V, \tag{4}$$

being c and n characteristic constants of the material.

This model bases on two main assumptions: i) viscous effects are localized at the edge of the contact line; ii) detachment occurs under constant pull-off rate conditions.

In eq. (3), the parameter β is proportional to the pull-off rate $V = -d\delta/dt$, while n may be determined experimentally. In general, n ranges from 0.1 to 0.8 (Muller, 1999). The initial value $\bar{a}(\bar{\delta})$ to solve eq. (3) is returned by JKR equations, which can be rewritten in dimensionless form as

$$\bar{a} = \left\{\frac{1}{2}\left[1+\left(1+\bar{F}\right)^{1/2}\right]\right\}^{2/3} \tag{5}$$

$$\bar{\delta} = \left(\bar{a}^2 + \frac{\bar{F}}{2\bar{a}}\right) \tag{6}$$

where $\bar{F} = F/F_0$ and $F_0 = 1.5\pi R\Delta\gamma_0$. The dimensionless contact load is then calculated by

$$\bar{F} = 2\bar{a}\left(\bar{\delta} - \bar{a}^2\right). \tag{7}$$

FT discrete model returns the value F_i of each contacting asperity, being F_i the load reached at the end of the loading process; eqs. (5) and (6) can hence be used to calculate the values of the contact radius a_i and penetration δ_i at the beginning of the unloading

phase.

In the experiments, unloading is performed by reducing the mean penetration Δ of the indenter in the rough surface at controlled displacement rate. A micro-asperity is assumed to jump out of contact when a critical jump-off distance is reached. Contrary to JKR theory, jump out of contact occurs always at zero contact area.

III. RESULTS AND DISCUSSION

In order to apply Muller's model for each detaching micro-asperity, we have to calculate the parameters n and c of eqs. (3-4). As shown in Violano et al. (2021), both parameters are scale independent. Their value can be hence obtained from contact tests on smooth PDMS by fitting the experimental data with the classical equation of Gent and Schultz (Gent and Schultz, 1972) relating the energy release rate G to the viscoelastic losses at the crack tip

$$G = \Delta\gamma_0[1 + c \cdot {v_c}^n]. \tag{8}$$

In particular, as shown in Fig. 5 of Violano et al. (2021), the best fit is obtained using $n = 0.25$ and $c = 31(\mathrm{m/s})^{-0.25}$. Unloading experiments have been performed at three different driving velocities ($V = 0.2$, 2, 20 μm/s). Due to the compliance of the cantilever beam supporting the spherical indenter, the actual velocity V_{act} is lower than the imposed value and it is equal to about $0.8V$ (Violano et al., 2021). The corresponding values of the parameter β are 0.00679, 0.0679, 0.679 μm/s.

Figures. 2A-C show the true contact area A as a function of the applied force F for three values of the detachment rate. Experimental tests are performed on rough patterns with asperities heights normally distributed with standard deviation $\sigma = 5$ μm.

Open and closed symbols refer to loading and unloading experimental data, respectively. Vertical and horizontal error bars show scattering of results obtained on 6 different experiments, corresponding to 6 contact realizations. Numerical predictions of the loading phase are plotted with black dashed line, while solid lines are used for the unloading phase.

Profilometry measurements showed that the vapor treatment used to smoothening the PMMA mold do not induce any change in the standard deviation of the asperity height distribution. However, it results in a roughly 10% increase in the radius of curvature of

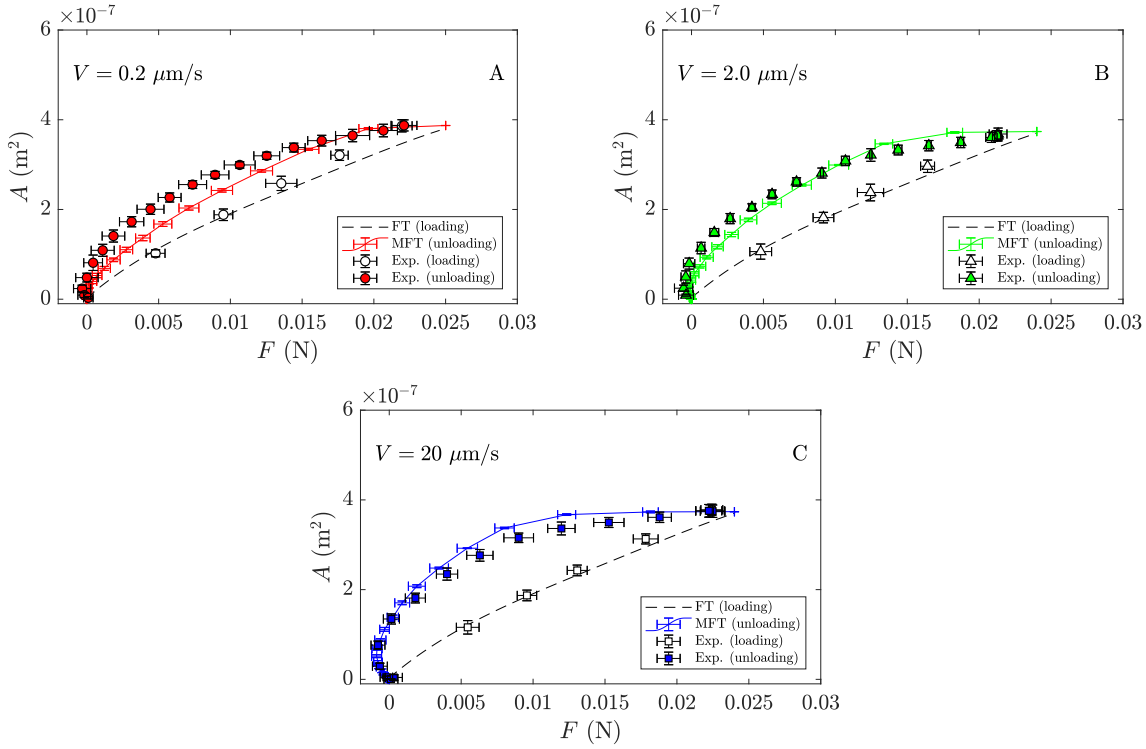

FIG. 2: Actual contact area A as a function of the applied load F. Results are obtained on rough patterns with $\sigma = 5$ μm and for (A) $V = 0.2$ μm/s, (B) $V = 2$ μm/s, and (C) $V = 20$ μm/s. In all cases unloading starts after reaching the load $F_{\max} = 0.025$ N. Experimental data are denoted with markers (open and closed symbols refer to loading and unloading phases, respectively). Error bars denote the standard deviation on 6 different realizations. Lines refer to numerical predictions. Loading curves are obtained with the discrete version of FT multiasperity model (FT), while the unloading ones are obtained by implementing the Muller's solution in the model to take into account viscoelastic dissipation (MFT).

some asperities. For this reason, contact simulations have been carried out on 5 numerically generated surfaces with random distributions of asperities radius of curvature. Specifically, the radius of curvature has been assumed ranging from 100 μm to 110 μm, with an average value of 105 μm. The numerical results dispersion is shown by the error bars on the solid lines.

A good agreement is found between experimental data and numerical predictions. The pull-off process is strongly influenced by the detachment rate V and, as expected, the pull-off force is enhanced by increasing V.

Figures 3A-C show the effect of the maximum applied preload $F_{\max}$ on the relation between contact area and applied load. Experimental tests are performed on rough patterns with $\sigma = 5$ μm, for a fixed unloading detachment rate $V = 2$ μm/s and for $F_{\max} = 0.012$,

0.025, 0.035 N. Once again we observe a quite good agreement with numerical predictions.

Figure 3D shows the variation of the load F with the rigid displacement Δ as predicted by the numerical model. As shown in the inset of the figure, the pull-off force is found to be almost independent of the point at which unloading starts. Increasing $F_{\max}$ of a factor ~ 3 leads to a 74% increase in the energy loss for adhesion hysteresis. In the contact of smooth elastic bodies, JKR theory predicts the pull-off force to be independent of $F_{\max}$. This result is still valid for viscoelastic media. In the case of rough contacts, it is not completely understood how surface roughness affects the dependence of the pull-off force on the maximum applied load. Recent experimental investigations (Dorogin et al., 2017) show the pull-off force increases with $F_{\max}$. However, such findings disagree with tests on rough PDMS performed by Kesari et al. (2010), which found a little, almost negligible, enhancement of the pull-off force with $F_{\max}$ in agreement with the Greenwood's statement: "*...in a number of calculations the pull-off force has proved to be almost, or completely, independent of the point at which unloading starts, although the initial parts of the curve certainly do differ.*" (Greenwood, 2017).

Figures 4A-C show the area-load curves during loading and unloading phases for three values of σ ($\sigma = 0$, 5, 10 μm). Unloading tests were performed at fixed detachment rate $V = 0.2$ μm/s. The agreement between experiments and numerical data is generally quite good. Figure 4D shows how the $F - \Delta$ relation changes with the roughness amplitude. We notice that the pull-off force vanishes when increasing σ, in agreement with the findings of Fuller and Tabor (1977) and Acito et al. (2019).

However, recent experimental works find that roughness may increase adhesion. Indeed, in contact tests between a spherical tip and PMDS with nanometer scale roughness, Kesari et al. (2010) found an 'optimal roughness' value, which maximizes the hysteretic energy loss.

Moreover, Dalvi et al. (2019) performed adhesion measurements on soft elastic PDMS hemispheres in contact with polycrystalline diamond rough substrates. Loading-unloading tests were conducted under quasi-static conditions, i.e., at very small values of the driving velocity of the indenter. The authors found that, even with negligible viscous effects, adhesion hysteresis still occurs because of the roughness-induced increase in contact area, in agreement with the predictions of the model of Persson and Tosatti (2001). Moreover, Greenwood extended the FT model to the unloading phase and found adhesion hysteresis

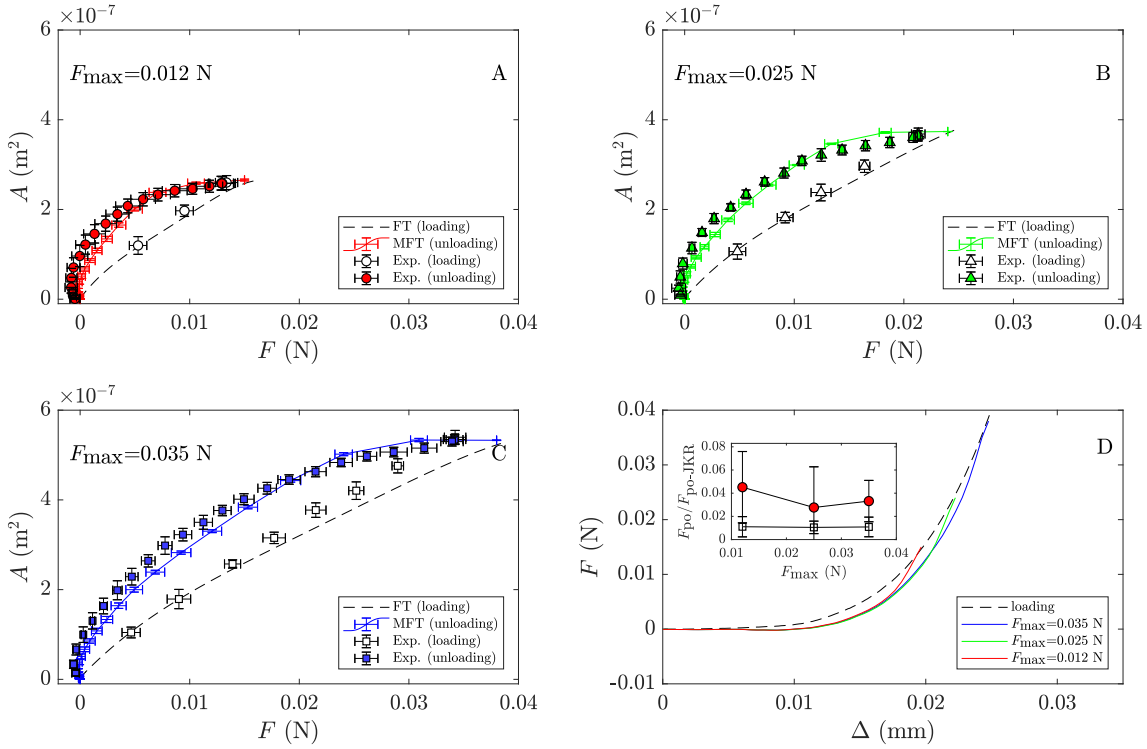

FIG. 3: Actual contact area A as a function of the applied load F. Results are obtained on rough patterns with $\sigma = 5$ μm and for $V = 2.0$ μm/s. Moreover, different values of the maximum applied preload are considered: (A) $F_{\max} = 0.012$ N, (B) $F_{\max} = 0.025$ N, and (C) $F_{\max} = 0.012$ N. Experimental data are denoted with markers (open and closed symbols refer to loading and unloading phases, respectively). Error bars denote the standard deviation on 6 different realizations. Lines refer to numerical predictions, obtained by FT model (loading) and MFT model (unloading). D) The load F as a function of the rigid displacement Δ of the indenter. Lines refer to numerical predictions. In the inset, the normalized pull-off force $F_{\rm po}/\ F_{\rm po-JKR}$ as a function of F_{max}; red circles and empty squares denote experimental and numerical data, respectively.

occurs also in absence of viscous effects because of elastic instabilities (Greenwood, 2017).

A. Hysteretic dissipation

For a rigid smooth sphere approaching a flat compliant substrate, the loading and unloading paths predicted by JKR theory and Muller model are shown in Fig. 5A. In JKR theory (black line), loading and unloading curves overlap and hysteretic energy loss (yellow area) is related to the elastic instabilities due to the different penetrations at which jump to contact (δ_{IN}) and detachment (δ_{OFF}) occur. In practical cases, such energy loss is usually negligible. On the contrary, in presence of viscous effects, the unloading path (red line) is

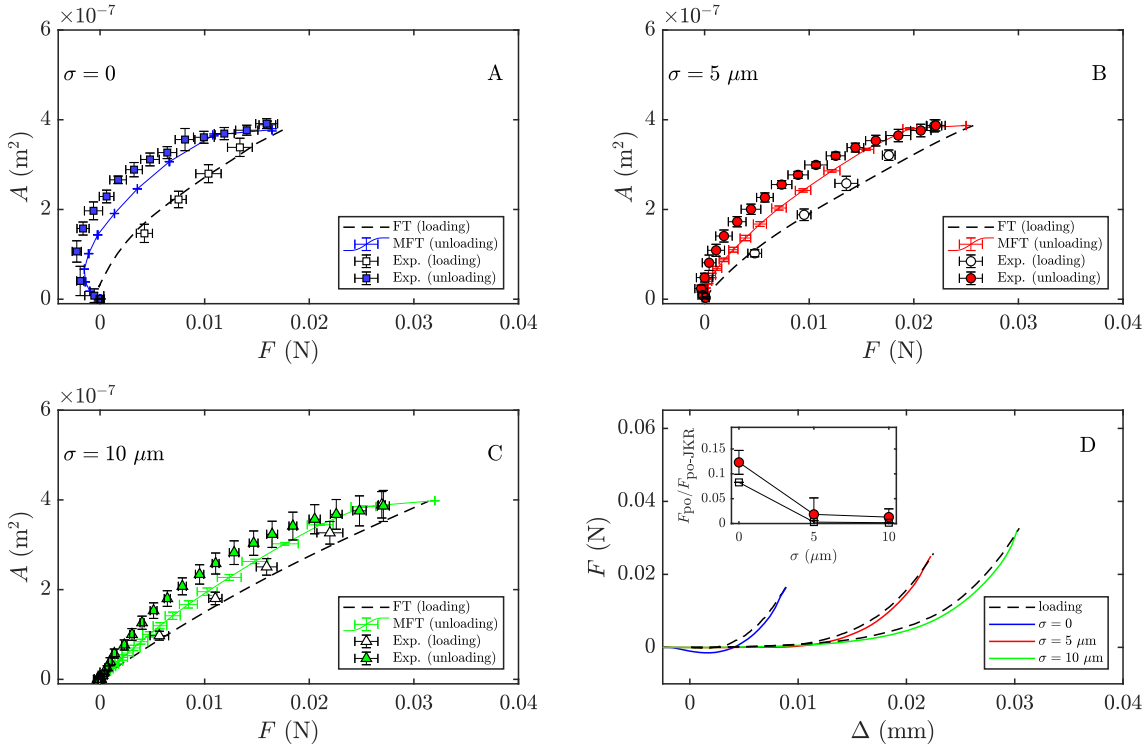

FIG. 4: The real contact area A as a function of the applied load F. Results are obtained on rough patterns with $\sigma = 0$ (A), $\sigma = 5$ μm (B), $\sigma = 10$ μm (C), and for $V = 0.2$ μm/s. Experimental data are denoted with markers (open and closed symbols refer to loading and unloading, respectively). Error bars denote the standard deviation on 6 different contact realizations. Lines refer to numerical predictions, obtained by the FT (loading) and MFT (unloading) models. (D) Load F as a function of the rigid displacement Δ of the indenter. Lines refer to numerical predictions. In the inset, the normalized pull-off force $F_{\rm po}/\ F_{\rm po-JKR}$ as a function of σ; red circles and empty squares denote experimental and numerical data, respectively.

rate-dependent and the hysteretic energy loss is much larger.

When a distribution of micro-asperities is textured on the substrate, the loading-unloading curves modify as shown in Fig. 5B. Numerical predictions are shown for $\sigma = 5$ μm. Negligible hysteresis occurs when viscous effects are neglected, demonstrating that the origin of adhesion hysteresis in our experiments is strongly related to viscoelasticity. However, when roughness is characterized by several length scales, larger elastic adhesion hysteresis can occur as experimentally shown in Dalvi et al. (2019). Furthermore, roughness with several length scales may also enhance localized phenomena of elastic instability (Carbone et al., 2015).

In our experiments, surface roughness reduces the pull-off force by a factor ~ 120 as we

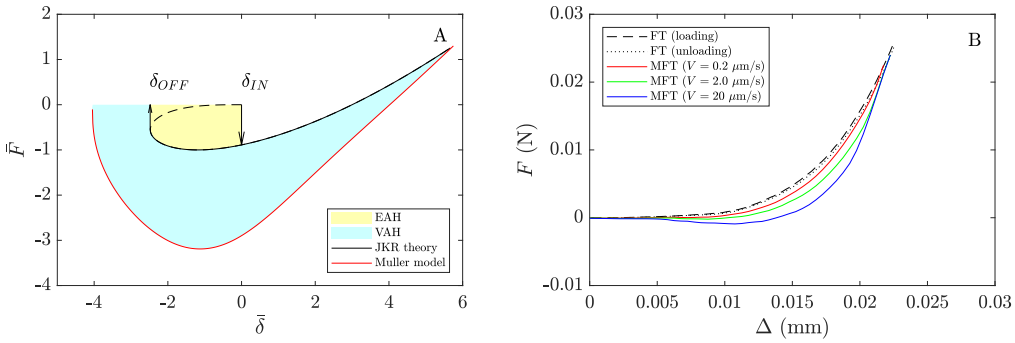

FIG. 5: (A) The force-approach relation for smooth elastic spheres, as predicted by the JKR and Muller models. The yellow and cyan areas represent the energy loss due to elastic instabilities (EAH) and viscoelastic dissipation (VAH), respectively. (B) Applied load F as a function of the rigid displacement Δ of the indenter as predicted by the theoretical model. The loading path is plotted with black dashed lines (FT model); the unloading elastic path is plotted with black dotted line (FT model); the unloading viscoelastic path is plotted with colored solid lines (MFT model). Results are obtained on rough patterns with $\sigma = 5$ μm and for $V = 0.2$, 2.0, 20 μm/s (red, green and blue).

deduce comparing results given in Figs. 6A and 6B. Specifically, in Fig. 6A, the estimated pull-off force $F_{\rm po}$ on rough PDMS is plotted in terms of the driving velocity V, while in Fig. 6B similar curves are given for the case of smooth sample. Notice $F_{\rm po}$ is normalized with respect to the pull-off force $F_{\rm po-JKR} = 1.5\pi R\Delta\gamma_0$ given by JKR theory. Results show an increase of $F_{\rm po}$ with V and a good agreement between experimental and numerical predictions (both at macro and microscales).

Tiwari et al. (2017) performing contact experiments on stiff PDMS ($E^* \sim 2$ MPa) observed that roughness leads to a decrease in $\Delta\gamma_{\rm eff}$ of a factor ~ 700. However, for very soft PDMS ($E^* \sim 0.02$ MPa) they found an enhancement of $\Delta\gamma_{\rm eff}$. The latter was observed close to full-contact conditions because of the roughness-induced increase in the real contact area. In our experiments we are far from full-contact conditions and this explains why we do not observe any increase in pull-off force moving from smooth to rough contact.

Moreover, pull-off force and effective surface energy are expected to be influenced by viscous dissipation. Specifically, we can identify two main mechanisms regulating changes in effective surface energy and, hence, contact area (Krick et al., 2012). One is the asperity-induced elastic energy which reduces adhesion on rough surfaces. In such case, elastic energy is stored at the interface helping to break adhesive bonds. For this reason, contact area is usually observed decreasing with increasing roughness. However, there is a second

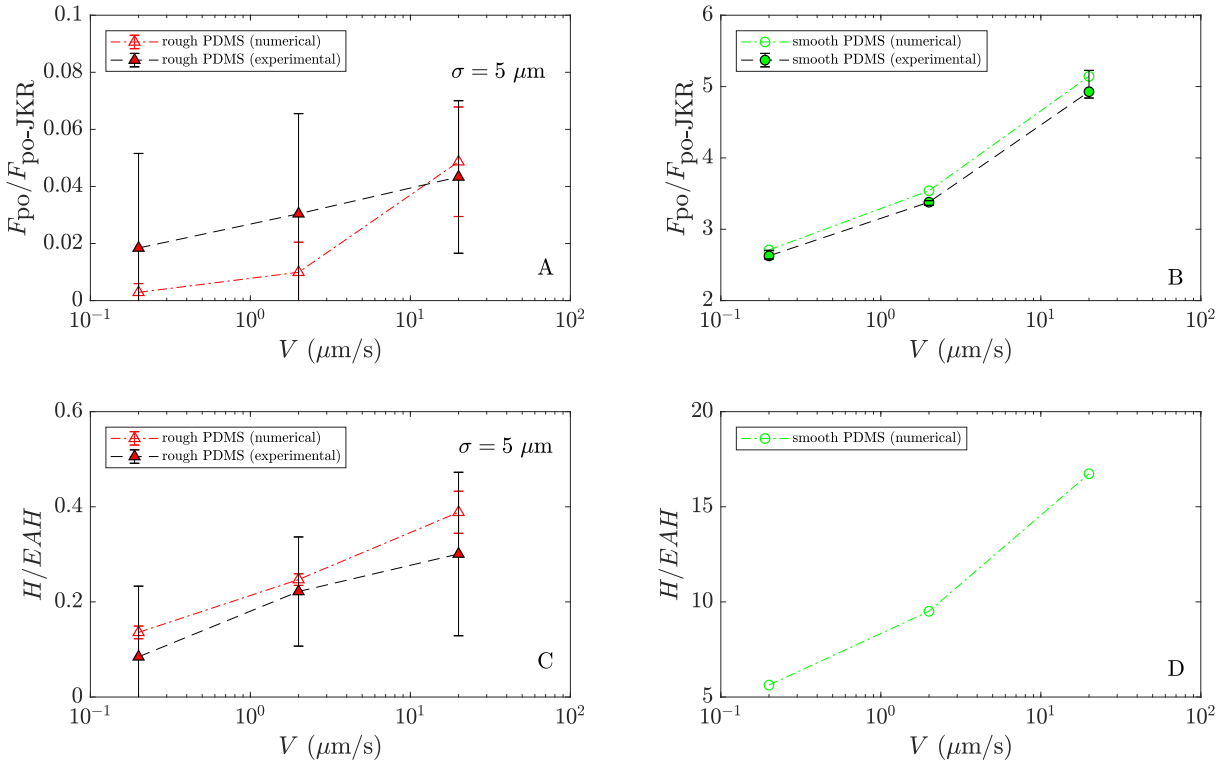

FIG. 6: (A) The normalized pull-off force $F_{\rm po}/F_{\rm po-JKR}$ for rough PDMS samples. Numerical (open triangles) and experimental (filled triangles) data are shown for $\sigma = 5$ μm and $V = 0.2$, 2.0, 20 μm/s. (B) The normalized pull-off force calculated for smooth PDMS samples. (C) The normalized hysteretic loss H/EAH obtained on rough PDMS samples. EAH is the energy dissipated as a result of the elastic instabilities predicted by the JKR theory for smooth contacts. (D) The normalized hysteretic loss calculated for smooth PDMS samples.

mechanism which instead entails an increase in the contact area. In fact, if we formulate the adhesive detachment as a problem of opening cracks, for viscoelastic materials there may be an increase in the effective interfacial energy due to viscous dissipation. This effect is significant for materials with a high glass transition temperature, which behave highly dissipative already for relative low velocities. However, this is not the case for PDMS which shows a low glass transition temperature ($T_g \approx -120$ °C). For this reason, we can expect the first mechanism dominates on the latter. Moreover, there is another reason for which we do not observe any increase in the effective surface energy. The opening crack propagation mechanism is proportional to the perimeter L of the boundary line separating contact from non-contact regions. For a smooth surface we have L_M scales as A/D, where A is the contact area and D its diameter. For a rough surface, L_m scales as A/d, where d is the

typical diameter of a contact spot. Therefore, for a randomly rough surface, we expect $L_m \gg L_M$ and surface roughness can enhance the contribution from the opening crack to the change in contact area. However, once again, this is not our case as we are considering roughness with only one length of scale. In fact, under a compressive load $F = 0.02$ N, we find that the total perimeter L_m of micro-contact spots is of the same order of magnitude of the perimeter L_M of the smooth macro-spot ($L_m \approx 2L_M$). On the contrary, the asperity-induced elastic energy stored at the interface induces a more significant reduction in contact area A (by a factor of ~ 31) thus governing the variation of $\Delta\gamma_{\text{eff}}$ in agreement with that observed by Israelachvili et al. (2000): "*...the effective adhesion force or surface energy per unit area can be very low - often many orders of magnitude below the value for two molecularly smooth surfaces - and is determined by a few isolated asperity contacts of low radii of curvature*".

The surface roughness is expected to have the same effect on hysteretic losses in agreement with previous observations given in Szoszkiewicz et al. (2006), who performing measurements of adhesion hysteresis at nanometer and micrometer length scales on mica, calcite, and metallic samples, found that hysteretic losses decrease of two orders of magnitude moving from micro to nano sized particles.

In this regard, the hysteretic loss occuring during a loading-unloading cycle is proportional to the area H enclosed between the loading and unloading curves shown in Fig. 5B. Its variation with the driving velocity V is plotted in Fig. 6C, where H is normalized with respect to the value calculated for a smooth sample in absence of viscous dissipation. In Fig. 6D the same plot is given for the case of smooth substrate. A great reduction in adhesion hysteresis is observed when experiments (and numerical simulations) are carried out on rough samples as a result of the decrease in the real contact area. Moreover, the hysteretic losses increase with the contact line velocity (and hence the driving one $V = v_c/(da/d\delta)$) as it affects dissipation within the crack tip zone.

IV. CONCLUSIONS

In this work, we performed experimental and numerical investigations on the adhesive normal contact between a spherical indenter and viscoelastic rough substrates.

The proposed numerical model makes use of a discrete version of the FT multiasperity

model to describe the loading phase and the solution proposed by Muller (Muller, 1999) to characterize the unloading one. Moreover, as we can also perform the unloading process neglecting viscous effects, we can distinguish the hysteretic energy loss due to viscous dissipation from that due to the roughness-induced increase in contact area.

Both experimental and numerical results show adhesion is strongly enhanced by increasing the detachment rate and decreasing the rms roughness amplitude, while the pull-off force is negligibly affected by the maximum applied load. This last trend is in agreement with previous studies (Greenwood, 2017; Kesari et al., 2010) but it seems to contradict the increase in pull-off force observed in Dorogin et al. (2017). However, we have to pointed out that our calculations are performed on simplified rough surfaces characterized by a single length scale.

Furthermore, we find that the increase in the effective adhesion energy with the contact line velocity is independent of the size of the radius of curvature, but it exclusively depends on the viscoelastic properties of the bodies. Interestingly, the increase in the perimeter of the contact line observed on rough samples negligibly affects the effective adhesion energy $\Delta\gamma_{\text{eff}}$, which is instead strongly affected by the reduction in contact area that, in our experiments, is therefore the parameter governing the change in surface energy observed when moving from smooth to rough samples.

The present study has limitations related to the simplistic description of the surface roughness, which usually presents fractal features. However, we believe it can be useful in clarifying some key points in the adhesion hysteresis of rough soft media ("*Asperity approach leads naturally to an understanding of the difference between loading and unloading, and so to why there is hysteresis*", Greenwood, 2017).

Acito, V., Ciavarella, M., Prevost, A.M., Chateauminois, A., 2019. Adhesive Contact of Model Randomly Rough Rubber Surfaces. Tribol. Lett. 67(2), 54. https://doi.org/10.1007/s11249-019-1164-9

Barthel, E., Frétigny, C., 2009. Adhesive contact of elastomers: Effective adhesion energy and creep function. J. Phys. D. Appl. Phys. 42(19), 195302. https://doi.org/10.1088/0022-3727/42/19/195302

Bauer, C.T., Kroner, E., Fleck, N.A., Arzt, E., 2015. Hierarchical macroscopic fibrillar adhesives: In situ study of buckling and adhesion mechanisms on wavy substrates. Bioin-

spiration and Biomimetics. 10(6), 066002. https://doi.org/10.1088/1748-3190/10/6/066002

Benedek, I., 2004. Pressure-sensitive adhesives and applications. CRC Press. https://doi.org/10.1201/9780203021163

Carbone, G., Pierro, E., Recchia, G., 2015. Loading-unloading hysteresis loop of randomly rough adhesive contacts. Phys. Rev. 92(6), 062404. https://doi.org/10.1103/PhysRevE.92.062404

Dalvi, S., Gujrati, A., Khanal, S.R., Pastewka, L., Dhinojwala, A., Jacobs, T.D.B., 2019. Linking energy loss in soft adhesion to surface roughness. Proc. Natl. Acad. Sci. U. S. A. 116(51), 25484-25490. https://doi.org/10.1073/pnas.1913126116

Deng, W., Kesari, H., 2019. Depth-dependent hysteresis in adhesive elastic contacts at large surface roughness. Sci. Rep. 9(1):1–12. https://doi.org/10.1038/s41598-018-38212-z

Dorogin, L., Tiwari, A., Rotella, C., Mangiagalli, P., Persson, B.N.J., 2017. Role of Preload in Adhesion of Rough Surfaces. Phys. Rev. Lett. 118(23), 238001. https://doi.org/10.1103/PhysRevLett.118.238001

Dorogin, L., Tiwari, A., Rotella, C., Mangiagalli, P., Persson, B.N.J., 2018. Adhesion between rubber and glass in dry and lubricated condition. J. Chem. Phys. 148(23), 234702. https://doi.org/10.1063/1.5025605

Fuller, K. N. G., Tabor, D., 1975. The effect of surface roughness on the adhesion of elastic solids. Proc. R. Soc. London. A. Math. Phys. Sci. 345(1642), 327-342. https://doi.org/10.1098/rspa.1975.0138

Gent, A.N., Schultz, J., 1972. Effect of Wetting Liquids on the Strength of Adhesion of Viscoelastic Materials. J. Adhes. 3(4), 281-294. https://doi.org/10.1080/00218467208072199

Greenwood, J. A., Williamson, J. P., 1966. Contact of nominally flat surfaces. Proc. R. Soc. London. Ser. A. Math. Phys. Sci. 295(1442), 300-319. https://doi.org/10.1098/rspa.1966.0242

Greenwood, J.A., 2017. Reflections on and Extensions of the Fuller and Tabor Theory of Rough Surface Adhesion. Tribol. Lett. 65(4), 159. https://doi.org/10.1007/s11249-017-0938-1

Haiat, G., Barthel, E., 2007. An approximate model for the adhesive contact of rough viscoelastic surfaces. Langmuir. 23(23), 11643-11650. https://doi.org/10.1021/la701560n

Israelachvili, J., Giasson, S., Kuhl, T., Drummond, C., Berman, A., Luengo, G., Pan,

J.M., Heuberger, M., Ducker, W., Alcantar, N., 2000. Some fundamental differences in the adhesion and friction of rough versus smooth surfaces. Tribol. Ser. 38, 3-12. https://doi.org/10.1016/s0167-8922(00)80107-8

Johnson, K. L., Kendall, K., Roberts, A. D., 1971. Surface energy and the contact of elastic solids. Proc. R. Soc. London. A. Math. Phys. Sci. 324(1558), 301-313. https://doi.org/10.1098/rspa.1971.0141

Kesari, H., Doll, J.C., Pruitt, B.L., Cai, W., Lew, A.J., 2010. Role of surface roughness in hysteresis during adhesive elastic contact. Philos. Mag. Lett. 90(12), 891-902. https://doi.org/10.1080/09500839.2010.521204

Krick, B.A., Vail, J.R., Persson, B.N.J., Sawyer, W.G., 2012. Optical in situ micro tribometer for analysis of real contact area for contact mechanics, adhesion, and sliding experiments. Tribol. Lett. 45(1), 185-194. https://doi.org/10.1007/s11249-011-9870-y

Lorenz, B., Krick, B.A., Mulakaluri, N., Smolyakova, M., Dieluweit, S., Sawyer, W.G., Persson, B.N.J., 2013. Adhesion: Role of bulk viscoelasticity and surface roughness. J. Phys. Condens. Matter. 25(22), 225004. https://doi.org/10.1088/0953-8984/25/22/225004

Maugis, D., Barquins, M., 1978. Fracture mechanics and the adherence of viscoelastic bodies. J. Phys. D. Appl. Phys. 11 1989–2023 https://doi.org/10.1088/0022-3727/11/14/011

Menga, N., Afferrante, L., Demelio, G.P., Carbone, G., 2018. Rough contact of sliding viscoelastic layers: numerical calculations and theoretical predictions. Tribol. Int. 122, 67–75. https://doi.org/10.1016/j.triboint.2018.02.012

Muller, V. M., 1999. On the theory of pull-off of a viscoelastic sphere from a flat surface. J Adhes Sci Technol. 13(9), 999-1016.

Persson, B.N.J., Tosatti, E., 2001. The effect of surface roughness on the adhesion of elastic solids. J. Chem. Phys. 115(12), 5597-5610. https://doi.org/10.1063/1.1398300

Szoszkiewicz, R., Bhushan, B., Huey, B.D., Kulik, A.J., Gremaud, G., 2006. Adhesion hysteresis and friction at nanometer and micrometer lengths. J. Appl. Phys. 99(1), 014310. https://doi.org/10.1063/1.2159081

Tiwari, A., Dorogin, L., Bennett, A.I., Schulze, K.D., Sawyer, W.G., Tahir, M., Heinrich, G., Persson, B.N.J., 2017. The effect of surface roughness and viscoelasticity on rubber adhesion. Soft Matter. 13(19), 3602-3621. https://doi.org/10.1039/c7sm00177k

Violano, G., Cheateaumionis, A., Afferrante, L., 2021. Rate-dependent adhesion of vis-

coelastic contacts. Part I: contact area and contact line velocity within model randomly rough surfaces.

Violano, G., Afferrante, L., 2019a. Contact of rough surfaces: Modeling adhesion in advanced multiasperity models. Proc. Inst. Mech. Eng. Part J J. Eng. Tribol. 223(10), 1585-1593. https://doi.org/10.1177/1350650119838669

Violano, G., Afferrante, L., 2019b. Modeling the Adhesive Contact of Rough Soft Media with an Advanced Asperity Model. Tribol. Lett. 67(4), 119. https://doi.org/10.1007/s11249-019-1232-1

Violano, G., Afferrante, L., 2019c. Adhesion of compliant spheres: An experimental investigation, in: Procedia Structural Integrity. 24, 251-258. https://doi.org/10.1016/j.prostr.2020.02.022

Wei, Z., He, M.F., Zhao, Y.P., 2010. The effects of roughness on adhesion hysteresis. J. Adhes. Sci. Technol. 24(6):1045–1054. https://doi.org/10.1163/016942409X12584625925222

Yashima, S., Romero, V., Wandersman, E., Frétigny, C., Chaudhury, M.K., Chateauminois, A., Prevost, A.M., 2015. Normal contact and friction of rubber with model randomly rough surfaces. Soft Matter. 11(5), 871-881. https://doi.org/10.1039/c4sm02346c